KOHRA, K., MOLIÈRE, K., NAKANO, S. & ARIYAMA, M. (1962). *J. Phys. Soc. Jpn*, **17**, (Suppl. B-II), 82-85.

LAUE, M. VON (1948). *Materiewellen und ihre Interferenzen*, 2nd ed., p. 357. Leipzig: Akademische Verlagsgesellschaft.

LEHMPFUHL, G. & REISSLAND, A. (1968). *Z. Naturforsch. Teil A*, **23**, 544-549.

LEHMPFUHL, G. & UCHIDA, Y. (1986). *Proc. Electron Microsc. Soc. Am.* pp. 376-379. San Francisco Press, Inc.

MARTEN, H. & MEYER-EHMSEN, G. (1985). *Surf. Sci.* **151**, 570-584.

OSAKABE, N., TANISHIRO, Y., YAGI, K. & HONJO, G. (1980). *Surf. Sci.* **97**, 393-408.

SHANNON, M. D., EADES, J. A., MEICHLE, M. E. & TURNER, P. S. (1985). *Ultramicroscopy*, **16**, 175-192.

TAFTØ, J. & LEHMPFUHL, G. (1982). *Ultramicroscopy*, **7**, 287-294.

UCHIDA, Y., JÄGER, J. & LEHMPFUHL, G. (1984). Proc. 8th Eur. Congr. Electron Microsc., pp. 567-568.

UCHIDA, Y., LEHMPFUHL, G. & JÄGER, J. (1984). *Ultramicroscopy*, **15**, 119-129.

VOSS, R., LEHMPFUHL, G. & SMITH, P. J. (1980). *Z. Naturforsch. Teil A*, **35**, 973-984.

Acta Cryst. (1986). A**42**, 577-585

Pendellösung Radiation and Coherent *Bremsstrahlung*

BY J. C. H. SPENCE AND G. REESE*

Department of Physics, Arizona State University, Tempe, AZ 85287, *USA*

(*Received* 14 *March* 1986; *accepted* 10 *July* 1986)

Abstract

The spontaneous emission process, which is kinematically forbidden in vacuum, may occur for kilovolt electrons traversing thin crystals as a direct result of the dynamical diffraction process which Paul Ewald was amongst the first to understand. The history of this effect is briefly reviewed. New experimental results, and the relevant theoretical background, are given for the resulting monochromatic X-ray emission lines known as coherent *Bremsstrahlung* and channelling radiation. The fine structure of these lines in particular is discussed, and their effects on electron energy-loss spectra described.

1. Introduction

'Having Ewald's theory as an example, it was easy to develop the theory of electron diffraction', wrote Hans Bethe in 1981. Guided by Ewald's ideas, Bethe thus developed the modern theory of dynamical electron diffraction, in which the absence of a vector field affords considerable simplification (Bethe, 1928). At a recent American Crystallographic Association meeting, Ewald reminisced on how he had developed his theory during off-duty hours in a horse-drawn ambulance during the First World War (Ewald, 1916). The discovery of electron diffraction from crystals in 1927 provided the incentive for the application of Ewald's work to charged particles. This paper outlines the way in which Bethe's theory of electron diffraction has become the basis of the modern theory of *Bremsstrahlung* from electrons traversing crystalline targets. Only comparatively recently has it been fully appreciated how profoundly the effects of dynamical diffraction influence the theory of *Bremsstrahlung* product in crystals, and how intimately the two effects are related. In brief, whereas the conventional theory of *Bremsstrahlung* for isolated atoms (due to Bethe and Heitler) predicts an emission spectrum which is continuous in energy up to a certain cutoff, the modern theory of *Bremsstrahlung* for 'low'-energy (<2 MeV) collimated electrons traversing a crystalline target predicts a series of monochromatic X-ray emission lines, one for each reciprocal-lattice vector and extinction distance. Since the energies and intensities of the lines are related to crystal structure factors, the resulting families of lines, known as coherent *Bremsstrahlung* (CB) and channelling radiation (CR), contain a great deal of crystal structure information. In the modern view, both CB and CR result from spontaneous emission between Bloch wave states of the incident beam. Only by taking these states to be solutions of the full three-dimensional dynamical diffraction problem, which Paul Ewald was amongst the first to understand, can the relationship between CB and CR be fully understood.

The purpose of this paper is to present experimental evidence for 'type B' coherent *Bremsstrahlung* lines from a new longitudinal mode in the zone axis (axial) orientation from diamond, and to provide the relevant theoretical background needed for its interpretation using the language of dynamical electron diffraction. Particular emphasis is placed on the crystal structure information in CB and CR. We also discuss the fine structure of these lines and the form of the electron energy-loss spectra to be expected from the CB and CR processes.

Channelling radiation was observed for the first time in 1975 (Vorobiev, Kaplin & Vorobiev, 1975),

* Motorola, Government Electronics Group, Scottsdale, AZ 85251, USA.

0108-7673/86/060577-09$01.50

while work on CB has continued for about thirty years, following the early speculation of Williams (1935) and theoretical treatment of Uberall (1956). The first experimental observations of CB were those of Barbiellini, Bologna, Diambrini Palazzi & Murtas (1962), while low-energy results were first obtained by Korobochko, Kosmach & Mineev (1965). Practically all this work, however, has been done at very high particle energies (MeV-GeV) at which diffraction effects are obscured, and a classical model is often appropriate. Here we concentrate on recent new low-energy CB results, for the interpretation of which Ewald's and Bethe's ideas are critically important. For a general review of CR and CB, see Saenz & Uberall (1985). Channelling radiation has been extensively studied by the Aarhus group, among others (see Andersen, Erikson & Laegsgaard, 1981).

2. Simple models and line-broadening effects

We consider a kilovolt electron traversing a thin crystal in the Laue geometry (see Fig. 1). The electron, travelling with velocity $v = \beta c$, encounters atoms in the inclined planes **g** shown, at a frequency $\omega' = 2\pi v/L'$, where L' is the lattice spacing measured in the rest frame of the electron. The energy of CB emission in that frame is then

$$\varepsilon' = \hbar\omega' = 2\pi\hbar v/L'. \qquad (1)$$

Relativistic effects are included by replacing the 'foreshortened' lattice spacing L' by the value $L = \gamma L'$ (as measured in the laboratory frame), and incorporating the angular-dependent relativistic Doppler effect

$$\omega = \omega'/\gamma(1-\beta\cos\theta). \qquad (2)$$

Here $\gamma = (1-\beta^2)^{-1/2}$. Thus the CB energy observed in the laboratory frame from the moving electron source is $\varepsilon = \hbar\omega$, where

$$\varepsilon = hc\beta/L(1-\cos\theta). \qquad (3)$$

For an interatomic spacing in ångströms, and ε in keV, this becomes

$$\varepsilon = 12{\cdot}4\,\beta/L(1-\beta\cos\theta). \qquad (4)$$

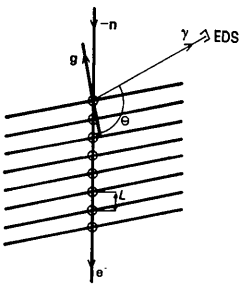

Fig. 1. Kilovolt electron traversing a thin crystal containing inclined planes **g**. Here L, θ and n are defined. An energy-dispersive X-ray spectrometer is indicated (EDS).

The angle θ is defined in Fig. 1. Thus there is an emission line for every periodic component of the electron's motion in this classical model, and we shall see that these are intimately related to the dynamical diffraction of the electron in a wave-mechanical picture. Fig. 2 shows an experimental CB spectrum recently obtained frrom 80 and 120 keV electrons incident along the [111] zone axis of diamond. The shift of the numbered peaks with accelerating voltage confirms that these are not characteristic X-ray emission lines. This spectrum was obtained using an energy-dispersive X-ray spectrometer (EDS) attached to a Philips EM400 electron microscope.

The peaks shown in Fig. 2 may be related to the reciprocal-lattice construction, since the distance between atoms along the beam path belonging to crystal planes **g** is $L = (\mathbf{g}\,.\,\mathbf{n})^{-1}$, where $-\hat{\mathbf{n}}$ is a unit vector in the beam direction. Defining $\boldsymbol{\beta} = (v/c)\hat{\mathbf{n}}$, the CB energy becomes

$$\varepsilon = hc\boldsymbol{\beta}\,.\,\mathbf{g}/(1-\beta\cos\theta). \qquad (5)$$

For low-energy CB the reciprocal-lattice vectors **g** which are important are those which are approximately antiparallel to the beam direction. While a more detailed theory includes a number of other factors, the predominant term in the CB energy depends on the component of the reciprocal-lattice vector in the beam direction. Thus emission due to different **g** vectors in the same reciprocal-lattice plane normal to the beam (not passing through the origin) will be of approximately equal energy. We adopt the loose but convenient definition of these planes as higher-order Laue zones (HOLZ). The plane passing through the origin (normal to the beam) is known as the zero-order Laue zone (ZOLZ). Fig. 3 shows the relevant projection of the diamond reciprocal lattice (not all points shown lie in the plane of the paper). For a beam direction **H**, **g** . **H** = n for reciprocal-lattice

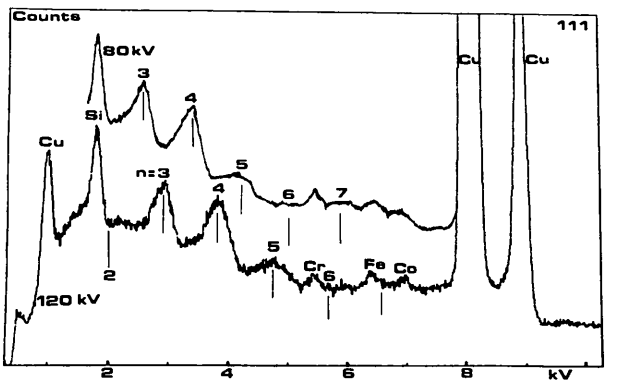

Fig. 2. Experimental CB spectra from the axial [111] orientation in diamond at 80 and 120 keV. Copper grid characteristic lines and detector fluorescence (Si) are also seen. The numbering gives the order of the Laue zones responsible. The peaks are asymmetrical, and vary with accelerating voltage, unlike characteristic X-rays. Peaks 2 and 6 are absent (see text).

vector **g** in HOLZ plane n. Thus the peaks observed in Fig. 2 can be assigned values of n according to the HOLZ responsible, as shown.

We note that peaks $n=2$ and $n=6$ are absent. These reciprocal-lattice planes satisfy the condition $h+k+l=2p$ (p odd) for absent reflections in the diamond lattice. This absence of CB peaks for HOLZ planes for which all structure factors are zero demonstrates convincingly the crystallographic and diffraction effects underlying the theory of CB. These absent lines are 'predicted' by the theory to be given in §6.

It is traditional to distinguish two forms of radiation, CB, discussed in simple form above, and channelling radiation (CR). In the language of dynamical electron diffraction, CR corresponds to the case where $L=\xi_g$ is a dynamical extinction distance (in simple cases). [A more refined model (see §3) is, however, needed to understand the details of CB and CR fine structure.] Hence CR occurs at lower energies than CB (in the UV for electron microscope voltages).

Thus, while CB may be thought of loosely as 'juddering' or dipole radiation with the dipole axis parallel to the beam, CR or '*Pendellösung*' radiation is more similar to the transverse 'wiggler' radiation used in synchrotrons. [A Bloch wave treatment of CR can be found in Spence & Humphreys (1984).] Thus CB would be most intense at right angles to the beam, were it not for the relativistic searchlight effect, which sweeps the intensity forward to an angle of approximately $\theta=1/\gamma$ (for large γ). The axial CB intensity is zero in the forward direction.

A final simple connection between CB and CR can be made as follows. Equation (5) is an approximation to the more accurate result

$$\varepsilon = hc\beta S_{\mathbf{g}}/(1-\beta\cos\theta) \qquad (6)$$

where $S_{\mathbf{g}}$ is the excitation error for reciprocal-lattice vector **g** in the plane $n (n\neq 0)$. The height of this plane above the ZOLZ is g_z, as required in (5). In the two-beam dynamical electron diffraction theory, $S_{\mathbf{g}}\simeq \xi_g^{-1}$ for large $S_{\mathbf{g}}$, so that CB could perhaps be thought of as 'weak-beam' *Pendellösung* radiation. Since the excitation errors are approximately equal to the reciprocals of the crystal stacking sequence in the beam direction, a connection is also made with the 'forbidden reflection' or termination reflection method of imaging surface steps in transmission electron microscopy.

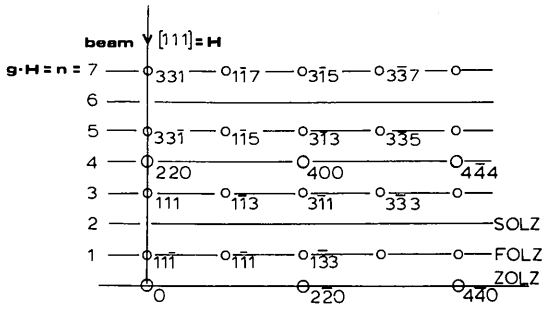

Fig. 3. Reciprocal lattice for the diamond structure. The numbered higher-order Laue zones correspond to the peaks in Fig. 2. Not all the points shown lie in the plane of the page.

In addition to line broadening owing to the many reciprocal-lattice vectors which may contribute to each peak, there is a Doppler broadening owing to the variation of emission energy across the detector semi-angle $\Delta\theta$. From (3), for a detector at $\theta=90°$, this is

$$\Delta E/\varepsilon = \beta\Delta\theta. \qquad (7)$$

A further line-broadening mechanism results from the limited depth for which the coherent elastic portion of the beam electron is excited. This wave field is depleted as a result of the activation of all the elementary excitations of the crystal, such as plasmons, phonons and atomic ionization. Of these, by far the most important 'dechannelling' mechanism is phonon excitation, since this may involve large-angle inelastic scattering. It can be shown that the line broadening ΔE arising from this effect is given by (3), with L replaced by

$$\Gamma = (\mu^j+\mu^i)/\pi, \qquad (8)$$

where μ^j and μ^i are the absorption coefficients for the two dominant Bloch waves. These are simply related to the imaginary parts of the 'optical' potential used in electron diffraction. If this absorption length is much greater than the crystal thickness t, the broadening is again given by (3), but with L replaced by t. For silicon, using 1 MeV electrons, we then find the thermal broadening to be about 1·25 eV at room temperature and 1·0 eV at 20 K, using the values of μ^i measured by Voss, Lehmpfuhl & Smith (1980). Thus the effects of cooling a sample to reduce the line width are minimal, because of the relatively large zero-point lattice vibration energy. This has important implications for the various attempts to use CB and CR as the basis for an electron 'laser'. The final line-broadening mechanism has been called 'Bloch wave broadening', and forms the subject of § 5 of this paper. For our experimental conditions, the magnitudes of these line-broadening effects, in decreasing order (for kilovolt electrons), are (1) Doppler broadening, (2) **g** vector broadening, (3) Bloch wave broadening, and (4) thermal broadening. The energy resolution of the X-ray detector must also be considered.

Since the emission energy in (5) is proportional to β, we see that CB provides a tunable source of X-rays in the soft X-ray region. To the extent that a single set of planes can be encouraged to dominate the process, the radiation is also polarized, with the electric field vector parallel to **g**. The intensity of CB is found to be about 3% of that of the copper $K\alpha$ line at 100 kV; however, this result depends on many things, including specimen thickness (Williams, 1986).

3. Spontaneous emission in crystals

Consider the spontaneous emission of a photon by an electron in vacuum. Energy and momentum conservation require that

$$m_e c^2 = (h^2 c^2 k_e^2 + m_e^2 c^4)^{1/2} + hcq, \qquad (9)$$

where q is the photon wave vector, k_e the electron wave vector and m_e the electron mass (all in the electron rest frame). This equation cannot be satisfied. For an electron traversing a thin crystal, however, two related effects make spontaneous emission possible - Bragg diffraction (or *Umklapp*) and dynamical dispersion. Although these effects are linked through the crystal potential, there are useful approximations which make it possible to associate the first of these (*Umklapp*) with the spontaneous emission responsible for CB and the second with CR. Loosely, we may say that the crystal provides something for the electron to 'kick against'. By modifying the dispersion surface from that of a free electron, dynamical diffraction makes possible spontaneous emission transitions which would otherwise be forbidden. However, we have already seen that this vacuum transition is forbidden. For CR these transitions are of the interband type and occur between the innermost dispersion surfaces shown in Fig. 4 (see Hirsch, Howie, Nicholson, Pashley & Whelan, 1977). For a given energy change only this transition involves a smaller momentum change than that which would occur between the 'vacuum spheres' (shown dashed) *in vacuo*. For CB we will see that, since the dipole approximation cannot be made at low accelerating voltages (the photon wave vector may be larger than a reciprocal-lattice vector), the usefulness of the distinction between interband and intraband transitions is largely lost. For small q, however, the CB transitions are of the intraband type.

If (9) is replaced by a momentum conservation law expressing conservation of *crystal* momentum,

$$\mathbf{k}^{i'} = \mathbf{k}^{j} + \mathbf{g} - \mathbf{q} \qquad (10)$$

and dispersion of the Bloch wave vectors $\mathbf{k}^j$ (for the initial state) and $\mathbf{k}^{i'}$ (for the final state) are allowed for by introducing

$$-\lambda^{i} = K^2 - k^{(j)2} \qquad (11)$$

and

$$-\lambda^{i'} = K'^2 - k^{(i')2} \qquad (12)$$

then spontaneous emission becomes possible. Here $\mathbf{K}$ ($\mathbf{K}'$) is the wave vector of the initial (final) state of the beam electron outside the crystal. The quantities $\lambda^{i'}$ and λ^{j} describe the deviation of the dynamical electron dispersion surface from the spheres which describe a free electron. The discrete nature of this allowed momentum transfer *in crystals* accounts for the monochromatic form of CB emission (for a point detector). This momentum transfer appears as a whole-body translation of the crystal, much as in the Mössbauer effect. The dispersion is responsible for CR and the fine structure on CB lines. When these equations are combined with the relativistically correct energy conservation laws, the emission energy measured in the laboratory frame is found to be (Reese, Spence & Yamamoto, 1984)

$$\varepsilon = hcq = hc\beta[g_z - g^2/2K - (\lambda^j - \lambda^{i'})/2K]/(1 - \beta\cos\theta) \qquad (13)$$
$$\varphi = 90°.$$

Here θ and φ are the angles q makes with $\mathbf{K}$ and $\mathbf{g}$ respectively, and $\lambda^{i'}$ and λ^{j} are eigenvalues obtained from solutions to the *three-dimensional* dynamical diffraction problem. These are inversely proportional to extinction distances. Since

$$S_{\mathbf{g}} = g_z - g^2/2K, \qquad (14)$$

equation (13) recovers (6) for $\lambda^j = \lambda^{i'} = 0$. The last two terms in (13) describe CR, while the first two describe CB. At the exact Bragg condition $S_{\mathbf{g}} = 0$, and pure CR results. In general, however, one has a mixture of transitions, involving combinations of these processes. Equation (13) shows the two types of line broadening mentioned earlier - the many values of g in a single HOLZ layer which contribute to a single peak in Fig. 2, while further broadening arises from the CB sidebands from the λ^j terms. These are discussed further in §5.

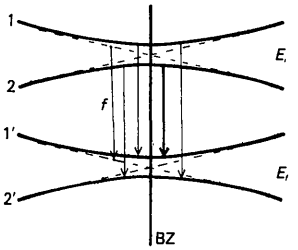

Fig. 4. CR transitions between Bloch wave states of initial energy E_i (1,2) and final-state energy E_f (1', 2'). Only the interband transition 2-1' shown bold involves less momentum transfer than the (forbidden) transition shown as f between free-electron states, whose dispersion surfaces are shown dashed. States 1 and 2 correspond to the same total energy (similarly for 1', 2'). See Hirsch, Howie, Nicholson, Pashley & Whelan (1977). BZ is the Brillouin zone boundary.

4. Dispersion surfaces

Our recent work has chiefly concerned a new type of longitudinal mode in CB, in which the momentum transfer g to the lattice may lie strictly antiparallel to the beam direction (*e.g.* peak $n = 3$ in Fig. 2). These transitions are only possible because of the variation of the crystal potential in the beam direction - thus they provide dramatic evidence of the failure of the projection approximation commonly used in dynamical electron diffraction. This case has been analyzed in detail theoretically by Kurizki (1986). It is instruc-

tive to consider these transitions as represented on the dynamical dispersion surfaces. These surfaces show the locus of $\mathbf{k}^i$ (which label the Bloch waves excited in the crystal) for a given total energy. All Bloch waves of the initial state correspond to the same total energy. The surfaces shown in Fig. 5 are those for GeAuAs, whose structure has recently been determined by electron diffraction (Vincent, Bird & Steeds, 1985). Continuous lines show the 'surfaces' for the initial state, while the dashed lines indicate surfaces of lower energy for the final state. Bloch waves are excited at points *A*, *B*, *C etc.* for the initial state. The kinematics of (10) are indicated.

Bolder lines (on the locus of a sphere passing through *A*) indicate the locus of strongly excited Bloch waves for the initial state. Since the energy and direction of the emitted photon is fixed for a given point on the spectrum and detector geometry, the termination point of q is fixed for *Umklapp* on a specified **g**. The figure shows the case of *Umklapp* on **g** antiparallel to a zone-axis beam direction, with an X-ray detector at right angles to the beam. The CR side bands then correspond to vertical movement of the family of final-state dispersion surfaces allowing **q** to terminate on different branches $\lambda^{i'}$. Strongly excited Bloch waves lie close to the bold 'vacuum sphere'; thus our numerical calculations suggest that it is a good approximation to consider only transitions out of the $n=2$ initial state of *A*. Then the spectrum of final states associated with a particular *Umklapp* g reflects the series of gaps between dispersion surfaces for the final-state diffraction conditions. These gaps open up at the Brillouin zone boundaries shown as the crystal potential is 'switched on', much as in the nearly-free electron theory of crystal electron-band structure. Note, however, that in that theory each Bloch wave eigenstate corresponds to a *different* total electron energy. Unfortunately, it is only in the soluble two-beam dynamical theory that these gaps are simply related to crystal structure factors or Fourier coefficients of crystal potential.

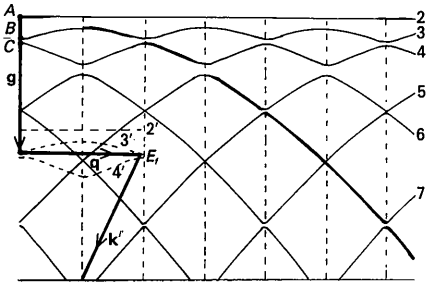

Fig. 5. Axial CB transitions represented on the dispersion surfaces for AuGeAs [see Vincent, Bird & Steeds (1985)]. Vertical dashed lines indicate the Brillouin zone boundaries, horizontal dashed lines are the final-state dispersion surfaces of energy E_f. In a scale diagram, the momentum transfer to the lattice g would be much larger. CR side bands on CB lines correspond to the termination point of g moving, for example, from 3′ to the lower branch 4′ shown.

We can conclude that, in principle at least, the fine structure of CB emission contains information on the eigenvalues of the crystal structure matrix (Spence, 1981). Since these eigenvalues are proportional to the sideband energies (which can be measured very accurately), their determination from CB spectra would avoid the problems of background subtraction which accompany any intensity measurement. However, no observations of fine structure on CB lines owing to dynamical dispersion have yet been reported, and the problems of distinguishing this line-broadening mechanism from the others discussed in §2 above are unlikely to be overcome soon. In current research, we have fitted a wavelength-dispersive X-ray spectrometer to a transmission electron microscope in order to study this fine structure.

The special case $\mathbf{q}=\mathbf{h}$ (*Umklapp* **g** antiparallel to axial **K**, **g** orthogonal to **q** and **h**) is of some interest. Here the emitted X-rays satisfy the Bragg condition with an X-ray Bragg angle of 90° for planes h containing the beam direction, which act as mirror reflectors. The resulting evanescent X-ray wave field set up in the crystal may enhance the photon intensity sufficiently to lead to stimulated emission from the electron beam. Closed-form results for this case have recently been obtained (Reese, Spence & Yamamoto, 1984). For cubic crystals, the conditions $\gamma=2^{1/2}$ (corresponding to an accelerating voltage of 211·66 kV) and [100] beam direction with $\theta=90°$ for the $\mathbf{h}=(022)$ crystal planes. Our recent experiments with silicon under these conditions failed to detect any enhancement of the (400) CB peak under this 'resonance' condition. This difficult experiment requires the absolute orientation of the target crystal with $\mathbf{h}=$ [022] in the X-ray detector direction and $\mathbf{g}=$[100] in the electron source direction.

5. Side bands and fine structure

The calculation of *Bremsstrahlung* emission intensities has traditionally been based on a two-step model involving intermediate states and plane-wave functions. This approach, however, is inadequate for the calculation of CR intensities, or for the calculation of CR 'side band' effects on CB spectra, in which dynamical dispersion is also important. [For a reconciliation of these approaches, see Andersen, Erikson & Laegsgaard (1981).] In the more accurate approach in which the emission is treated as spontaneous emission between Bloch wave states of the three-dimensional crystal potential, the intensity in the laboratory frame for a thin crystal can be written (Reese, Spence & Yamamoto, 1984)

$$\frac{\mathrm{d}P}{\mathrm{d}\Omega}=\frac{\alpha^3 a^2 \hbar\omega_r^2 T}{2\pi\gamma^4\beta c(1-\beta\cos\theta)^3}|\mathbf{q}\times\mathbf{M}|^2 \qquad (15)$$

where $\mathrm{d}P$ is the energy emitted per incident electron

into solid angle $d\Omega$, T is the crystal thickness, α is the fine-structure constant, a the Bohr radius, and $\mathbf{q}$, $\mathbf{M}$ and ω are measured in the rest frame (all other quantities are in the laboratory frame). The matrix element $\mathbf{M}^{ij}$ is given by

$$\mathbf{M}^{ij} = \frac{2\pi i}{\tau}\sum_{gg'} \alpha^j C_g^j C_{g'}^{i'*}(\mathbf{k}_r^j+\mathbf{g}_r)\delta(\mathbf{k}_r^j+\mathbf{g}_r-\mathbf{k}_r^{i'}-\mathbf{g}_r'-\mathbf{q}_r)$$
$$= \sum_{\mathbf{h}} \mathbf{M}_{\mathbf{h}}^{ij} \qquad (16)$$

where

$$\mathbf{M}_{\mathbf{h}}^{ij} = \frac{2\pi i}{\tau}\sum_{\mathbf{g}} \alpha^j C_{\mathbf{g}}^j C_{\mathbf{g}-\mathbf{h}}^{i'*}(\mathbf{k}_r^j+\mathbf{g}_r)\delta(\mathbf{k}_r^j+\mathbf{h}_r-\mathbf{k}_r^{i'}-\mathbf{q}_r) \qquad (17)$$

with all quantities measured in the rest frame ($C_{\mathbf{g}}$ is independent of frame). Each value of $\mathbf{h}$ corresponds to a different *Umklapp* process (for CB), with $\mathbf{h}=0$ describing CR.

Using the linearized eigvenvalue method of Dederichs (1971), we have evaluated (15) for a variety of cases. The three-dimensional eigenvalue problem must be solved separately for both the initial and final states. Since $q > g$, these may refer to entirely different diffraction conditions, and no symmetry reduction is possible. For example, an initial state $\mathbf{k}^j$ in axial channelling conditions, coupled to a final state $\mathbf{k}^{i'}$ in planar conditons, is conceivable. For the calculation of the profile of a single peak in Fig. 2, the sum over $\mathbf{h}$ extends over the relevant HOLZ, while that over $\mathbf{g}$ includes all of reciprocal space for which the Debye-Waller factor is appreciable. Our Fourier coefficients of crystal potential V_g were obtained from the electron scattering factors of Doyle & Turner (1968). An efficient perturbation method has also been suggested (Howie, 1984).

Fig. 6(a) shows the computed intensity profile for the sixth-order Laue zone in diamond with a [114] electron-beam direction at 120 kV. The intensities in Fig. 6(a) are computed on a simple plane-wave model (Reese, Spence & Yamamoto, 1984), in which the intensity from each possible *Umklapp* $\mathbf{g}$ is proportional to $|\mathbf{g}_z . V_{\mathbf{g}}|^2$. An X-ray detector resolution of 2 eV is assumed. The photons emerge with the component of their wave vector perpendicular to the beam direction parallel to [22$\bar{1}$]. Two of the *Umklapp* $\mathbf{g}$ contributing are labelled. These labels refer to the reciprocal-lattice vector $\mathbf{g}$ in (13). Fig. 6(b) shows the result of an exact many-beam Bloch wave calculation for the same case, indicating the effects of the dispersion of the wave field and consequent Bloch wave 'side bands' and line broadening. This fine structure is not seen in the experimental spectrum (Fig. 2) owing to the limited energy resolution of energy-dispersive detectors (about 150 eV). Finally, Fig. 6(c) shows the more realistic case where a detector resolution of 20 eV is assumed, corresponding to the new spectrometer under trial at ASU. We see that the applicability of the plane-wave theory depends, amongst other things, on the energy resolution of the detector used. Bloch-wave effects cannot be seen at low energies using energy-dispersive X-ray detectors.

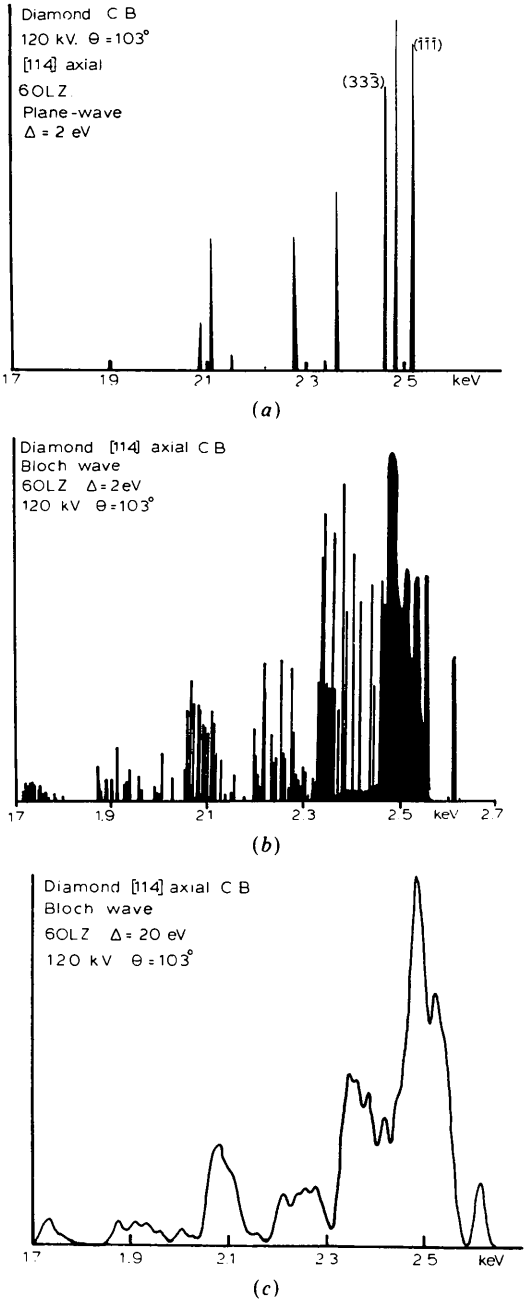

Fig. 6. (a) The calculated axial CB emission spectrum for diamond at 120 kV ($\theta = 103°$) using a plane-wave model, with a [114] beam direction. A detector energy resolution of 2 eV has been assumed, allowing individual peaks to be assigned Miller indices (two are indicated). All peaks arise from the sixth-order Laue zone. (b) Similar to (a), except that a full three-dimensional Bloch wave calculation has been employed. Here CR 'side bands' and other modifications result from the dispersion of the Bloch waves. (c) Similar to (b). However, the detector energy resolution has been increased to 20 eV. The detector semi-angle is assumed small in these calculations (negligible Doppler broadening).

Since the fine structure of CB lines depends on the three-dimensional diffraction conditions of the final state, the detailed shape of these lines is found to depend on the azimuthal direction of the X-ray detector. Thus, as a crystal is rotated about the crystal zone axis (and collinear beam direction), the fine structure of CB lines is predicted to change. Experiments to observe this effect at 0·8 MeV have been unsuccessful owing to limited detector energy resolution.

It has been suggested that, whereas CR corresponds to transitions between the transverse bound states of the projected crystal potential, CB corresponds to transitions between free (plane-wave) states. Our calculations show that whereas the predominant Bloch wave for the initial state in axial CB is deeply bound, the final state may be either bound or free. In general, at low energies where dispersion is strong the three-dimensional Bloch wave functions cannot be separated into a simple product of transverse and longitudinal components, so that the bound or free distinction is less useful.

A simple estimate of the separation of Bloch wave side bands on axial CB lines may be made for the special case of a final state at the two-beam Bragg condition. Then $\lambda^2 \sim 0$ and

$$hc\beta\lambda^{2',3'}/2K = \pm V_g. \tag{18}$$

Thus for a detector at right angles to the beam ($\theta = 90°$), the side band splitting is, from (13),

$$\Delta\varepsilon = 2V_g. \tag{19}$$

We note that this simple result is dependent on the two-beam approximation for the final-state dispersion - CB cannot easily, therefore, be used to measure Fourier coefficients of crystal potential. Equation (19) does, however, give some estimate of the energy resolution needed to observe Bloch wave effects on CB spectra. The limitation on angular width imposed by (7) then makes problems of background reduction severe.

6. Electron energy-loss spectroscopy of CB and CR

We now consider the possibility of observing effects corresponding to CB and CR emission in the transmitted-beam electron energy-loss spectrum. This technique offers at first sight the important advantages of superior energy resolution (about 1 eV) and greater collection efficiency, since most of the electrons suffering *Bremsstrahlung* energy losses fall within the collection angle of the energy-loss spectrometers fitted to modern electron microscopes. In addition, the energy range covered (0–2 kV) complements that of energy-dispersive X-ray detectors. Unfortunately, the angular integration performed by most spectrometers means that a single peak is not seen in the energy-loss spectrum, since electrons are collected from photons emitted in all directions. The form of the energy-loss spectrum can be estimated by modelling CB emission as arising from a classical dipole oscillator, oscillating in the beam direction. For CR we may assume a transverse dipole, and in both cases make the dipole approximation and integrate the result over all angles. Then the shapes of the electron energy-loss spectra in the laboratory frame may be shown to be (Reese, Spence & Yamamoto, 1984)

$$dN/dE \simeq [(E_{lab}/\gamma\varepsilon') - 1]^2\beta^{-2} \quad \text{for CR} \tag{20}$$

$$dN/dE \simeq \{1 - [(E_{lab}/\gamma\varepsilon') - 1]^2\}\beta^{-2} \quad \text{for CB.} \tag{21}$$

Here, dN/dE is the number of beam electrons losing energy in the range E_{lab} to $E_{lab}+dE$, while ε' is the rest-frame emission energy [see (1)]. The maximum and minimum energy cutoffs correspond to photon emission at $\theta = 0$ and $\theta = 180°$ respectively. Fig. 7 shows these two energy-loss spectral shapes for 100 kV electrons. The difficulties in observing these shapes against the appreciable background of other processes are apparent, and our experiments to observe this effect in diamond and MgO have not been successful.

The possibility of angular selection in energy-loss spectroscopy is considered in Fig. 8. If Bloch wave effects are ignored, this shows the plane-wave kinematics for axial CB given by (10) on the Ewald sphere construction, with $\mathbf{K}$ and $\mathbf{K}'$ now replacing the Bloch wave vectors $\mathbf{k}^j$ and $\mathbf{k}^{i'}$. Equation (13) (with $\lambda^{i'} = \lambda^i = 0$) then describes an ellipse in three dimensions, whose eccentricity is approximately β. The 'inelastic Ewald sphere' of radius K' is also shown. Fig. 9 shows the locus of points on a transmission electron diffraction pattern for which the electron has lost a particular amount of energy. The electron energy-loss spectrum obtained from a point on these curves might be expected to show a single sharp peak, and experiments of this type are under way at ASU. The figures take no account of the finite resolution of the detectors. Similar energy-loss effects owing to transition radiation have been reported previously (Cowley, 1982). As a final possibility, we mention the use of

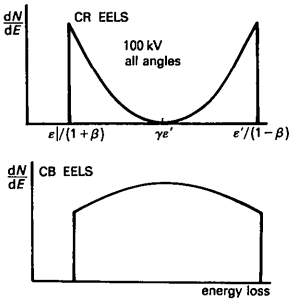

Fig. 7. Electron energy-loss spectral shapes expected for CR and CB using 100 keV electrons. A spectrometer which collects over a large angle has been assumed, and the emission is monochromatic in the rest frame.

coincidence counting between the energy-loss and photon-emission channels, which has recently been shown to be a practical possibility (Ahn & Krivanek, 1985).

7. Discussion

In this paper we have tried to show that dynamical diffraction, which Paul Ewald first understood in detail, has the most profound effect on the *Bremsstrahlung* emission spectrum from crystalline targets. These effects have only recently become fully understood, owing to the efforts of many researchers in many countries. Their applications (and those of closely related channelling effects) include particle identification in high-energy physics, the development of tunable polarized X-ray sources and the construction of compact particle extractors for accelerators. The unwanted effects of CB lines on the spectra used for the X-ray microanalysis of transmission samples have also been noted. Here the effect of crystallinity (which becomes increasingly important as electron probe sizes decrease) is seen to concentrate the otherwise continuous *Bremsstrahlung* background into peaks, and thereby set the ultimate detection limit for microanalysis by this technique. No similar effect can be expected in the microanalysis of bulk samples owing to the high background arising from other processes.

In a broader context it can be seen that the CB and CR from electrons at low accelerating voltages are but two modern electron diffraction effects in which the full translational symmetry of the beam electron and/or that of crystal electrons must be considered in order to predict the observed spectra. Thus, in the theoretical development of CB and CR, as in the development of the theory of electron energy-loss near-edge fine structure [Disko, Spence, Sankey & Saldin (1986); see also Taftø & Krivanek (1982) for the effects of electron channelling on characteristic energy losses], and that of electron channelling effects on characteristic X-ray production (Spence & Taftø, 1983), early models based on plane waves and isolated-atom wave functions have given way to more sophisticated models which allow for dynamical diffraction of both beam and crystal electrons.

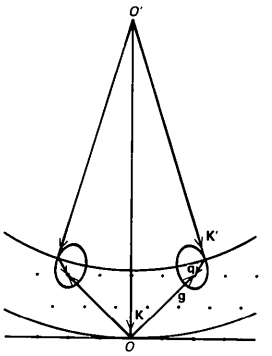

Fig. 8. Scattering kinematics for axial CB. In an angle-integrated energy-loss experiment all **g** vectors which terminate on the 'inelastic Ewald sphere' **K'** shown contribute to the spectrum at a given energy loss. Thus *Umklapp* on **g** vectors other than those shown (related by symmetry) may contribute to the electron energy-loss spectral intensity of a particular energy loss. The axis of the ellipse is directed towards *O'*.

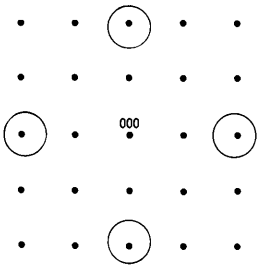

Fig. 9. These circles indicate schematically the locus of final-state electron wave vectors corresponding to a given energy loss owing to coherent *Bremsstrahlung*. This wave vector may also couple to other *Umklapp* events (not shown). The incident electron-beam direction is normal to the page, and the dots represent the transmitted electron diffraction spots of the initial state.

This work was supported by NSF grant No. DMR8512784 and the facilities of the NSF National High Resolution Electron Microscopy Center at ASU. We are most grateful to Drs J. Titchmarsh and J. Maguire for their generous assistance with this work.

References

AHN, C. & KRIVANEK, O. (1985). *Proc. Electron Microsc. Soc. Am.*, p. 406.

ANDERSEN, J. U., ERIKSON, K. R. & LAEGSGAARD, E. (1981). *Phys. Scr.* **24**, 588-600.

BARBIELLINI, G., BOLOGNA, G., DIAMBRINI PALAZZI, G. & MURTAS, G. P. (1962). *Phys. Rev. Lett.* **8**, 454-457.

BETHE, H. A. (1928). *Ann. Phys. (Leipzig)*, **87**, 55-129.

COWLEY, J. M. (1982). *Phys. Rev. B*, **25**, 1401-1404.

DEDERICHS, P. M. (1971). *Dynamical Diffraction Theory.* KFA-Jülich Report JUL-797-FF (Jülich). Kernforschungsanlage, Jülich.

DISKO, M., SPENCE, J. C. H., SANKEY, O. & SALDIN, D. (1986). *Phys. Rev. B*, **33**, 5642-5651.

DOYLE, P. & TURNER, P. (1968). *Acta Cryst.* A**24**, 390-397.

EWALD, P. P. (1916). *Ann. Phys. (Leipzig)*, **49**, 117-143.

HIRSCH, P. B., HOWIE, A., NICHOLSON, R. B., PASHLEY, D. W. & WHELAN, M. J. (1977). *Electron Microscopy of Thin Crystals*, 2nd ed., p. 446. London: Butterworths.

HOWIE, A. (1984). Personal communication.

KOROBOCHKO, YU. S., KOSMACH, V. F. & MINEEV, V. I. (1965). *Zh. Eksp. Teor. Fiz.* **48**, 1248-1256 [*Sov. Phys. JETP*, **21**, 834-839].

KURIZKI, G. (1986). *Phys. Rev. B*, **33**, 49-63.

REESE, G. M., SPENCE, J. C. H. & YAMAMOTO, N. (1984). *Philos. Mag.* **49**, 697-716.

SAENZ, A. W. & UBERALL, H. (1985). *Coherent Radiation Sources. Springer Verlag Topics in Current Physics*, Vol. 38. Berlin, New York: Springer-Verlag.

SPENCE, J. C. H. (1981). *Experimental High Resolution Electron Microscopy.* Oxford, New York: Oxford Univ. Press.

SPENCE, J. C. H. & HUMPHREYS, C. J. (1984). *Optik (Stuttgart)*, **66**, 225-242.

SPENCE, J. C. H. & TAFTØ, J. (1983). *J. Microsc. (Oxford)*, **130**, 147-154.
TAFTØ, J. & KRIVANEK, O. (1982). *Nucl. Instrum. Methods*, **194**, 153-158.
UBERALL, H. (1956). *Phys. Rev.* **103**, 1055-1067.
VINCENT, R., BIRD, D. & STEEDS, J. (1985). *Philos. Mag.* **A50**, 745-763.
VOROBIEV, A. A., KAPLIN, V. V. & VOROBIEV, S. A. (1975). *Nucl. Instrum. Methods*, **127**, 265-268.
VOSS, R., LEHMPFUHL, G. & SMITH, P. (1980). *Z. Naturforsch. Teil A*, **35**, 973-984.
WILLIAMS, D. B. (1986). Personal communication.
WILLIAMS, E. J. (1935). *K. Dan. Vidensk. Selsk. Mat.-Fys. Medd.* **13**, No. 4, 38-45.

SHORT COMMUNICATIONS

Contributions intended for publication under this heading should be expressly so marked; they should not exceed about 1000 *words; they should be forwarded in the usual way to the appropriate Co-editor; they will be published as speedily as possible.*

Acta Cryst. (1986). A**42**, 585-587

Extremely skew X-ray diffraction.

By H. R. HÖCHE and O. BRÜMMER, *Martin-Luther-Universität Halle-Wittenberg, Sektion Physik, Friedemann-Bach-Platz* 6, *DDR*-4020 *Halle, German Democratic Republic*, and J. NIEBER, *Martin-Luther-Universität Halle-Wittenberg, Sektion Geographie, Domplatz* 5, *DDR*-4020 *Halle, German Democratic Republic*

(*Received* 10 *February* 1986; *accepted* 1 *August* 1986)

Abstract

Skew reflections are becoming more and more important in X-ray surface diffraction. A geometrical discussion of the whole dispersion surface in extremely skew cases gives the angular ranges of incidence and emergence in which the condition of X-ray diffraction is fulfilled. The main intensity comes from the incidence range given by $|\chi_0-\chi_h|^{1/2}<\theta_i<|\chi_0+\chi_h|^{1/2}$, where χ_0 and χ_h are the Fourier coefficients of dielectric susceptibility of the crystal. Furthermore, the exit angle of the diffracted beam is of the order of the critical angle of specular total reflection.

1. Introduction

In the dynamical theory of X-ray diffraction starting from P. P. Ewald's and M. von Laue's work (*e.g.* von Laue, 1960) the discussion of the dispersion surface is useful for the interpretation of X-ray beams. Usually the dispersion surface is discussed in its section with the diffraction plane consisting of the incident beam, the exit beam and the diffraction vector $\mathbf{b}_h$. For nearly all relevant experiments checking the dynamical theory, so-called zero-layer diffraction is realized (*i.e.* the normal to the entrance surface lies in the diffraction plane). Diffraction experiments using skew reflections can be treated on the basis of the conventional theory only for small angles between the surface normal and the diffraction plane. Especially in the case of grazing incidence the dynamical theory must be extended in such a manner that the curvature of the spheres of incidence and emergence must be taken into account, as given by Rustichelli (1975). Starting with the work of Marra, Eisenberger & Cho (1979) a new technique was developed, the so-called X-ray surface diffraction. The dynamical treatment of these diffraction experiments was given by Afanas'ev & Melkonyan (1983) by means of the extended dynamical theory of X-ray diffraction given by Bedynska (1973, 1974), Brümmer, Höche & Nieber (1976*a*, *b*, 1979) and Härtwig (1976, 1977). The aim of this paper is the geometrical interpretation of the phenomena of X-ray surface diffraction on the basis of the three-dimensional dispersion surface.

2. The spatial dispersion surface

The beam geometry for skew X-ray reflections can be represented in a simple way. Generally all possible incident and exit beams are on cones with the diffraction vector $\mathbf{b}_h$ as axis. In this paper we consider only the case where the diffraction vector lies in the crystal surface. This geometry corresponds to a symmetrically skew Laue case. The term 'symmetrically skew' means that the incident and exit beams make the same angles with the crystal surfaces of a plane parallel crystal and exact fulfilment of the Bragg condition is realized. Extremely skew reflections can be characterized by small angles between the diffraction vector and the crystal surface and a small angle between the incident X-ray beam and the crystal surface.

For the wave vectors outside and inside the crystal the component parallel to the crystal surface must be constant. Geometrically that means that both wave vectors have their starting points on the same normal to the crystal surface. By means of a complete representation of the dispersion surface it is possible to determine the angular ranges, which are of interest for measurements in extremely skew geometry. In Fig. 1 an attempt at a three-dimensional picture of the dispersion surface is presented; only the spheres with radius $r=nk$ (inside the crystal, n = refraction index, k = vacuum wave number) are sketched and the two branches of the hyperbolic planes are partially drawn. In the upper part the discus-like surface is shown. In the lower part the other hyperbolic surface is sketched. For clarity only one polarization state is considered. The equatorial plane of the two spheres represents the crystal surface. The section of the dispersion surface containing this plane is the well known picture (see Fig. 2*a*), but here the wave

0108-7673/86/060585-03$01.50